Prediction of a large number of electron pockets near the band edges in type-VIII clathrate Si_{46} and its physical properties from first principles

2013 J. Phys.: Condens. Matter 25 475502

(http://iopscience.iop.org/0953-8984/25/47/475502)

IOP PUBLISHING JOURNAL OF PHYSICS: CONDENSED MATTER
J. Phys.: Condens. Matter **25** (2013) 475502 (9pp) doi:10.1088/0953-8984/25/47/475502

Prediction of a large number of electron pockets near the band edges in type-VIII clathrate Si_{46} and its physical properties from first principles

Payam Norouzzadeh[1], Charles W Myles[2] and Daryoosh Vashaee[1]

[1] Helmerich Advanced Technology Research Center, Oklahoma State University, Tulsa, OK 74106, USA
[2] Department of Physics, Texas Tech University, Lubbock, TX 79409-1051, USA

E-mail: payam.norouzzadeh@okstate.edu

Received 25 August 2013, in final form 30 September 2013
Published 31 October 2013
Online at stacks.iop.org/JPhysCM/25/475502

Abstract
The material design of type-VIII clathrate Si_{46} is presented based on first principles. The structural, electronic, elastic, vibrational, and thermodynamic properties of this hypothetical material are presented. Our results predict that type-VIII clathrate Si_{46} is an indirect semiconductor with a bandgap of 1.24 eV. The band structure revealed an interestingly large number of electron pockets near both conduction and valance band edges. Such a large density of states near the band edges, which is higher than that of the best thermoelectric materials discovered so far, can result in a large thermoelectric power factor (>0.004 W m^{-1} K^{-2}) making it a promising candidate for thermoelectric applications. The elastic properties as well as the vibrational modes and the phonon state densities of this material were also calculated. Our calculations predict that the heat capacity at constant volume (isochoric) of this clathrate increases smoothly with temperature and approaches the Dulong–Petit value near room temperature. The electronic band structure shows a large number of valleys closely packed around the valance band edge, which is rare among the known semiconducting materials. These valleys can contribute to transport at high temperature resulting in a possibly high performance (ZT $>$ 1.5) p-type thermoelectric material.

(Some figures may appear in colour only in the online journal)

1. Introduction

The lattice structures of clathrate materials based on Si, Ge, and Sn are formed by face-shared polyhedral cages of the group IV elements. Further these cages are often filled with alkali-metal, alkaline-earth or rare-earth atoms [1]. The pristine group IV clathrates, the guest-containing materials with only group IV atoms on the framework, and the materials with some host atom substitutions are all very interesting from both practical and basic physics considerations. In particular, for the clathrate materials, the choices of the guest atoms and the type and number of group II or group III atoms substituted on the framework may both be used to tune the material properties. This can result in a broad spectrum of possible electrical and transport properties for these materials. For example, depending on the host composition and on the guest atom choice, the Si-based clathrates can range from wide-gap semiconductors [2] to materials with metallic conduction [3], and to superconductors [4] (with Na or Ba guests).

Group IV clathrates typically simultaneously have very low lattice thermal conductivity ($\sim$1 W m^{-1} K^{-1} at room temperature) and high electrical conductivity (found in high carrier concentration metals with values greater than 6000 Ω cm). They are thus promising candidates to fulfil the phonon glass electron crystal (PGEC) criteria proposed by Slack as an indicator of an efficient thermoelectric

material [5]. Over the past several years, there has been considerable experimental and theoretical research in the search for better thermoelectric materials, and many of these studies have searched for materials with PGEC properties. Many materials with the potential for thermoelectric applications, including the clathrates, have cages containing guest atoms which vibrate (rattle) at very low frequencies ($\leq$50 cm^{-1}) [6] inside the cages (rattling structures). These low-lying modes are thought to resonantly scatter with the heat-carrying host acoustic phonons, thus lowering the thermal conductivity [7]. Because the guest atom–host atom bonding is weak, the presence of the guests usually has little effect on the host conduction bands, so that these materials have the potential to be good PGECs.

A relative comparison of the thermoelectric performance of materials can be obtained by comparing their dimensionless figures-of-merit $ZT = \alpha^2\sigma T/k$, where T is the absolute temperature, α is the Seebeck coefficient, σ is the electrical conductivity, and k is the thermal conductivity. At present, the best thermoelectric materials are semiconductors with narrow band gaps and low thermal conductivities. Of the several classes of materials which have been studied, the group IV clathrate materials have been shown to be among the materials with the highest ZT [8]. These clathrates usually have relatively large lattice constants which can cause short mean paths for phonon–phonon scattering and in turn lead to a reduced lattice thermal conductivity. Moreover, it is well known that not only the rattling atoms in the clathrate framework but also the open nature of the framework can lead to low lattice thermal conductivity [9].

Most of the experimental and theoretical studies of the group IV clathrates have focused on the type-I materials based on Si, Ge and Sn [1, 10–13]. Some of the group IV clathrates with the type-II structure have also been studied [14–16]. There are only five synthesized materials in the type-VIII clathrate family (space group: $I\bar{4}3m$), including $Ba_8Ga_{16}Ge_{30}$ [13], $Eu_8Ga_{16}Ge_{30}$ [17], $Sr_8Ga_{16-x}Al_xGe_{30}$ ($6 < x < 10$) [18], $Sr_8Ga_{16-x}Al_xSi_{30}$ ($8 < x < 10$) [19], and $Ba_8Ga_{16-x}Cu_xSn_{30}$ ($0 < x < 0.033$) [20]. Further, the first one transforms to a β-phase or type-I clathrate structure (space group: $Pm\bar{3}n$) above 696 C [1]. The type-VIII clathrates are expected to have high charge carrier mobility, which generally results in a high ZT [1, 21]. For example, a ZT $\approx$ 1.2 at 400 K was estimated by theoretical calculations for the $Eu_8Ga_{16}Ge_{30}$-VIII clathrate when optimally p-type doped [21]. The goal of our study is to provide basic inputs of Boltzmann transport theory such as lattice constant, bandgap, and other electronic structure and lattice dependent material parameters for further calculation of thermoelectric properties.

In this paper, we present results from first principles density functional calculations of the structural, electronic, vibrational, elastic and thermodynamic properties of the type-VIII clathrate Si_{46}. To our knowledge, this work is the first reported first principles theoretical study of Si_{46}-VIII clathrate which includes vibrational and thermodynamic properties. Also to our knowledge, this material is so far purely hypothetical. That is, none of them has yet been laboratory synthesized.

Our calculations are based on the generalized gradient approximation (GGA) to density functional theory. First, we have optimized the geometry of the lattice structure. The elastic constants (C_{ij}) of the selected clathrate were then studied and the relevant quantities were calculated. Based on those calculations, the Debye temperatures of this material were then predicted. We have also calculated the vibrational modes and the phonon state densities of this material and, have used the results of those calculations to predict some of their temperature-dependent thermodynamic properties.

2. Theoretical details

2.1. Lattice structure

The type-VIII clathrate crystallizes in the bcc lattice structure, with a guest-free unit cell containing 46 atoms. The unit cell structure consists of one kind of dodecahedral cage with small empty spaces in each cage. The general chemical formula for the ideal type-VIII clathrate structure is $A_8B_xC_{46-x}$ in which the A atoms are the guests residing in the host atom cages and B or C atoms are the host or framework atoms. We note that the chemical formula for the better-known type-I clathrate materials is identical to that for the type-VIII materials discussed here. However, the type-I clathrates crystallize on the SC lattice structure (space group $Pm\bar{3}n$ and international tables number 223). The type-VIII materials are thus distinguished from their type-I relatives by the fact that they crystallize in the bcc structure (space group $I\bar{4}3m$ and international tables number 217). There is only one kind of polyhedral framework for the guest atoms in type-VIII clathrates while two kinds of framework in type-I clathrates [1]. In both type-I and type-VIII structures, the host atom is bonded with four neighbor atoms by the sp^3 hybridizing orbital. All chemical formulas used in what follows refer to type-VIII materials.

The known type-VIII clathrate materials crystallize in the non-centro-symmetric space group $I\bar{4}3m$ (No. 217). Figure 1 depicts the configuration of atoms in a type-VIII clathrate unit cell. More details of the lattice structure of the type-VIII can be found in [1].

2.2. Density functional theory parameters

Our calculations are based on density functional theory (DFT) [22, 23] and use the GGA-PBE [24] exchange correlation functional. We have used a linear response approach [25–27], to compute vibrational properties of Si_{46}-VIII together with an iterative minimization, norm-conserving pseudopotential plane-wave method, as implemented in the ABINIT package [28]. These pseudopotentials are single projector, ordinary norm-conserving potentials, based on the Troullier–Martins method [29–31]. For Si atoms four valence electrons were used. The k-point sampling in the Brillouin zone and the plane-wave cutoff energy were tested to ensure that the absolute total energies converged to 3 meV/atom, and that the elastic constants converged to within 2 GPa. A 6 $\times$ 6 $\times$ 6 regular shifted k-point

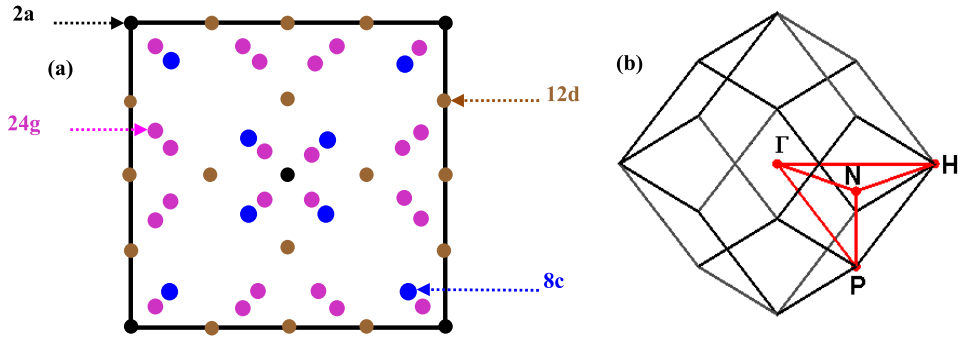

Figure 1. (a) Crystal structure of the guest-free type-VIII clathrate viewed along the *x*-direction. Host atoms occupy 2a, 12d, 8c, and 24g sites. (b) The first Brillouin zone of a typical type-VIII clathrate and the *k*-point path.

mesh and a 60 Ryd cutoff was defined for the plane-wave expansion. Brillouin zone integrations are carried out with a Methfessel–Paxton [32] smearing with a smearing parameter of 0.01 Ryd. We found that there was no appreciable change in the properties of interest when a 8 × 8 × 8 grid was employed in the calculations. For the phonon frequencies, we used a wavevector mesh of 8 × 8 × 8 to warrant a good coverage of the dispersion relations. The dynamical matrices were obtained from perturbation theory [26, 27]. A Fourier interpolation scheme was used to increase the mesh sampling in order to improve the description of quantities such as the vibrational density of states (VDOS), the heat capacity at constant volume, etc.

2.3. Structural optimization

The first step in our calculations was the optimization of the lattice geometry of the material. Structural optimization was carried out using Hellmann–Feynman forces and the Broyden–Fletcher–Goldfarb–Shanno-based method for the minimization of energy [33]. During the calculations, relaxations of both the internal structural parameters and the cell shape were included. To this end, we have chosen a fixed unit cell volume and have relaxed the atomic positions using atomic forces. This process was repeated for several different lattice constants until the global minimum energy was obtained for the material of interest. The structural relaxation was performed until the residual forces and stresses were less than 5×10^{-5} Hartree/bohr and 5×10^{-7} Hartree/bohr^3, respectively. The resulting GGA energy versus volume function has then been fitted to the Birch–Murnaghan equation of state[3] to obtain the equilibrium unit cell volume. Finally, the atom positions have relaxed at the equilibrium unit cell volume. The convergence was achieved within 1 cm^{-1} for the calculated phonon frequencies. Because the clathrate unit cell is very large (lattice constant ∼ 10 Å), a supercell which is a single unit cell was employed in all calculations.

[3] The Birch–Murnaghan equation for the energy E as a function of volume V is $E(V) = E_0 + 9/8(KV_0)[(V_0/V)^{2/3} - 1]^2\{1 + [(4 - K')/2][1 - (V_0/V)^{2/3}]\}$. E, E_0, V, V_0, K and K' are the energy, minimum energy, the volume, volume at the minimum energy, the bulk modulus and its pressure derivative respectively.

2.4. Elastic properties

Although the single crystal bulk modulus of a material can be easily calculated from the equation of state, a full set of single crystal elastic constants are needed in order to obtain mechanical properties. The elastic properties of a cubic crystal are determined by the three elastic stiffness constants C_{11}, C_{12}, and C_{44}. Calculation of elastic constants (C_{ij}) provides information about both mechanical stability and thermal transport properties of materials. For instance, given the Grüneisen parameter, the thermal expansion coefficient can be obtained [34]. Moreover, to calculate the lattice thermal conductivity according to extended Callaway method [35], having the values of Debye temperature, Grüneisen parameter, and longitudinal and transverse sound velocities which can be extracted from elastic constants is necessary. The ABINIT code provides these three constants C_{ij} [36]. The C_{ij} were obtained by straining the lattice at fixed volumes. Subsequently, the free energy was calculated as a function of the strain. Another method which is used to investigate efficiently the elastic properties of materials is the Le Page and Saxe least-squares method [37]. They use the calculated stresses as inputs to a least-squares fit of parameters in the stress–strain relationships for a selected series of strains in which are symmetry-unique and moduli are calculated from the first derivatives of the stresses. The three single crystal elastic constants of Si_{46} are listed in table 1. The single crystal bulk modulus B, and the tetragonal shear modulus C' are connected to the three independent C_{ij} as:

$$B = \frac{C_{11} + 2C_{12}}{3} \tag{1}$$

and

$$C' = \frac{C_{11} - C_{12}}{2}. \tag{2}$$

The shear modulus G can be obtained by the Hill polycrystalline modulus [38]:

$G_{\mathrm{H}} = 1/2(G_R + G_V)$, where the G_R and G_V are [39]:

$$G_R^{-1} = \tfrac{2}{5}C'^{-1} + \tfrac{3}{5}C_{44}^{-1} \tag{3}$$

Table 1. The predicted values of lattice constants, formation energies and bandgap for the type-VIII clathrate Si_{46} are summarized in table 1. Also, the DFT results for Si_{46}-I were presented for comparison.

Type-VIII clathrate	Si_{46}-VIII	Si_{46}-I[a]	Si_{46}-I[b]
Lattice constant (Å)	10.10	10.229	10.08
Formation energy (kJ mol^{-1})	7.84	6.01	7.255
Bandgap (eV)	1.24	1.314	1.3
Density (g cm^{-3})	2.081	2.004	2.098

[a] Our calculations.
[b] Reference [3].

and

$$G_V = \tfrac{2}{5}C' + \tfrac{3}{5}C_{44}. \tag{4}$$

Given the shear modulus, the factor of anisotropy C_a can be deduced to the following relation:

$$C_a = \frac{G}{C_{44}}. \tag{5}$$

Young's modulus E, E_{100} (along [100]), and E_{111} (along [111]) can be expressed as:

$$E = \frac{9BG}{3B+G} \tag{6a}$$

$$E_{100} = \frac{(C_{11}+2C_{12})(C_{11}-C_{12})}{(C_{11}+C_{12})} \tag{6b}$$

$$\frac{1}{E_{111}} = \frac{1}{E_{100}} + \frac{C_{11}-C_{12}-2C_{44}}{3C_{44}(C_{11}-C_{12})}. \tag{6c}$$

The longitudinal v_L and the transversal v_T sound velocities were calculated using the following relations [40]:

$$\rho v_L^2 = B + \tfrac{4}{3}G \tag{7}$$

and

$$\rho v_T^2 = G \tag{8}$$

where ρ is the density. The average speed of sound was obtained by:

$$v_s^{-3} = \frac{1}{3}\left(\frac{1}{v_L^3} + \frac{2}{v_T^3}\right). \tag{9}$$

Given the longitudinal and transversal velocities, the Debye temperature was calculated as [41]:

$$\theta_D = \frac{hv_s}{k_B}\left[\frac{3}{4\pi}\left(\frac{N_A\rho}{M}\right)\right]^{\frac{1}{3}} \tag{10}$$

where h, k_B, N_A, and M, are Planck's constant, Boltzmann's constant, Avogadro's number, and average molecular weight, respectively.

According to the Grüneisen–Debye approximation, determination of the Grüneisen's constant γ_G from the internal energy–volume equation of state was possible. An equation of state that incorporates Grüneisen's constant as a parameter is [42]

$$E(V) = \frac{BV_0}{\frac{5}{6}-\gamma_G}\left(\frac{V}{V_0}\right)^{\frac{5}{6}-\gamma_G}\left(\ln\frac{V}{V_0} - \frac{1}{\frac{5}{6}-\gamma_G}\right) + E_\infty \tag{11}$$

in which V_0 is the equilibrium volume. One definition of Grüneisen's parameter is:

$$\gamma_G = \frac{-V_0}{\theta_D}\frac{\partial\theta_D}{\partial V}. \tag{12}$$

This gives another way to calculate it. The numerical procedure consists of the calculation of the Debye temperature for two or more volumes which are close to the equilibrium volume and then applying the two point finite difference derivative or a higher-order derivative formula to get the Grüneisen parameter. It is notable that numerical errors are more likely in the latter procedure due to numerical derivative.

2.5. Phonon spectra

The ABINIT code is computationally demanding; however, it allows increasing the precision of the calculations. Therefore, for the calculation of the phonon spectra, we have employed the ABINIT implementation where the density functional perturbation theory (DFPT) was used. The phonon spectra and density of states are the two quantities we have calculated primarily for describing the vibrational properties of the type-VIII clathrate of interest. Lattice-dynamical calculations were performed to obtain the optimized structure. Linear response properties such as phonon frequencies were obtained as the second derivatives of the total energy with respect to atomic displacements within the framework of the DFPT. The linear response method allowed the calculation of the dynamical matrix at arbitrary wavevectors q. The force constants were extracted from a Fourier transform of the dynamical matrix obtained for a grid in the first Brillouin zone (BZ). These were later employed to obtain the phonon frequencies at arbitrary points in reciprocal space and the phonon dispersion relations by interpolation. The phonon spectra based on the interatomic force constants were obtained by Fourier interpolation with specific treatment of the long-range dipole–dipole interaction [26]. The phonon density of states was also calculated using these force constants by a tetrahedron method using a 8 × 8 × 8 grid [43, 44].

2.6. Thermodynamic properties

The thermodynamic properties of the clathrate Si_{46}-VIII were calculated using the harmonic approximation assuming that the system is a perfect crystalline lattice and that the only contribution to the entropy is the lattice vibrations. Anharmonic effects were assumed to be small because all vibrational eigenvalues were obtained at $T = 0$ K.

The vibrational Helmholtz free energy (F_{vib}), vibrational entropy (S_{vib}) and heat at constant volume (C_v) were calculated from vibrational density of states (VDOS). The procedure to obtain VDOS is outlined elsewhere [45].

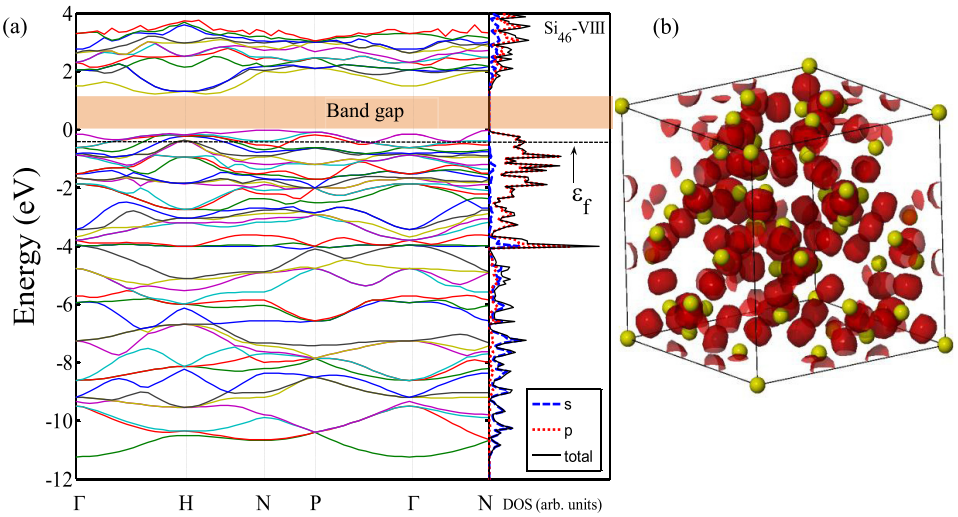

Figure 2. (a) GGA electronic band structure and scaled total density of states (DOS) for Si_{46}-VIII. The figure displays the energy bands along several symmetry directions of the first Brillouin zone. In units of $2\pi/a$, the labeled k points correspond to $\Gamma = (0, 0, 0)$, $H = (1/2, 1/2, -1/2)$, $N = (1/2, 0, 0)$ and $P = (1/4, 1/4, 1/4)$. The Fermi level is set to 0 eV and is shown by the horizontal dashed line. The dark salmon colored rectangle shows the bandgap. (b) Electron localization function ELF of Si_{46}-VIII.

Although experiments are generally conducted at constant pressure, it is still reasonably accurate to calculate the Helmholtz free energy rather than Gibbs energy. It should be mentioned that these free energies are not usually directly accessible in the experiment. The measurable quantities are mechanical quantities such as pressure, bulk quantities like volume and density, and thermal properties such as temperature and heat flow. In addition to the fact that we used equilibrium volumes in all our calculations, the thermal expansion coefficient is very small in semiconductors up to a few hundred degrees above room temperature. For example, in the diamond-structure Si, the thermal expansion coefficient is $\sim 4.68 \times 10^{-6}\ \mathrm{K}^{-1}$ at room temperature [46]. Thus, calculating the VDOS at 0 K and ignoring temperature dependence of the lattice constant is appropriate and it simplifies the calculation.

In the harmonic approximation, the vibrational Helmholtz free energy is given by:

$$F_{\mathrm{vib}}(T) = k_{\mathrm{B}}T \int_0^{\infty} \left[\tfrac{1}{2}\hbar\omega + k_{\mathrm{B}}T \ln\left(1 - \mathrm{e}^{-\frac{\hbar\omega}{k_{\mathrm{B}}T}}\right)\right] g(\omega)\, \mathrm{d}\omega \tag{13}$$

where k_{B} is the Boltzmann constant. It is notable that, although, the anharmonic effects are not considered at the level of the harmonic approximation, the thermal expansion is taken into account by introducing the effect of the temperature and the pressure in $F_{\mathrm{vib}}(T)$ [3]. The VDOS is normalized such that $\int g(\omega)\, \mathrm{d}\omega = 3N$, where N is the number of atoms. The zero point vibrational energy is defined by F_{vib} at $T = 0$ K. The vibrational entropy and the heat at constant volume are given by:

$$S_{\mathrm{vib}}(T) = \left(\frac{\partial F_{\mathrm{vib}}}{\partial T}\right)_V \tag{14}$$

and

$$C_V(T) = -T\left(\frac{\partial^2 F_{\mathrm{vib}}}{\partial T^2}\right)_V. \tag{15}$$

3. Results and discussion

An analysis of the electronic structure of the clathrate material discussed above can provide information about the effective masses, bandgap, and the multiplicity of the conduction and valence bands extrema, which are correlated with the electronic structure of the material. In fact, the large density of states effective mass leads to high Seebeck coefficient while the large conduction effective mass decreases the thermoelectric power factor [47]. Also, it is known that a multi-valleyed thermoelectric material is expected to exhibit a higher figure-of-merit than a similar material which possesses only a single valley [48]. Moreover, the bandgap indeed limits the peak ZT. At higher temperatures, the higher ZTs can be reached if the bandgap is increased while all other parameters remaining unchanged [49]. Following the structural optimization, we obtained a lattice constant of 10.10 Å for Si_{46}-VIII clathrate through calculation of the GGA minimum total energy as a function of volume and then by fitting the energy–volume data to the Birch–Murnaghan equation of state (see footnote 3). Our predicted electronic band structure and density of states for the clathrate of interest is plotted in figure 2. As can be seen in figure 2(a), due to the large number of atoms in the unit cell, the number of bands is very large (58 bands).

Due to the flatness of the bands which is signature of non-dispersive region for electrons in the Brillouin zone, especially near the Fermi level at the top of the valence band in this material, determination of the k-point to k-point transition for the minimum energy gap is difficult. We predict that the type-VIII clathrate Si_{46} should have an indirect bandgap between the Brillouin zone points $N = (1/2, 0, 0)$ and a k point between $\Gamma = (0, 0, 0)$ and $H = (1/2, 1/2, -1/2)$ points. The predicted GGA bandgap of the Si_{46} clathrate is approximately 1.24 eV. The bandgap value obtained for Si_{46} is much larger than that of diamond Si by about 0.7 eV. The total

width of the valence band is narrower than that of diamond Si by about 0.65 eV.

The band structure calculations also provide information about the effective masses and band non-parabolicity, which can be used in semi-classical transport models for the calculation of the charge carrier and phonon transport properties such as electrical conductivity, Seebeck coefficient, and thermal conductivity. Generally, a large effective density of states mass leads to a large Seebeck coefficient. Therefore, the multi-valley conduction and valence band characteristics of type-VIII clathrate Si_{46} are expected to result in large Seebeck coefficients for both n- and p-type materials. In the valance band, the degeneracies of $\Gamma(0, 0, 0)$, $N(1/2, 0, 0)$, and $P(1/4, 1/4, 1/4)$ points and along ΓH and NH lines are 1, 6, 2, 6, and 12, respectively. The top of the valance band is at N point. P, ΓH, NH, Γ valleys are located below the N point by 77.7 meV, 89.1 meV, 117.7 meV and 138.0 meV, respectively. For the conduction band, the band minimum is located at the ΓH line with a degeneracy of 6. The two minima at the NH line (12-fold degenerate) and the Γ point are located 2.7 meV and 262.7 meV above the edge, respectively. These valleys, which amount to total number of 27 for the valance band and 19 for the conduction band, contribute to transport at a high temperature when the thermal energy is comparable to their separation. Such a large number of closely packed valleys is higher than that of the best thermoelectric materials discovered so far. For example, the corresponding numbers for Bi_2Te_3 based thermoelectric alloys are 7 and 18 for the conduction and valance bands [50]. Therefore, Si_{46}-VIII is expected to result in a large thermoelectric power factor, which deserves further theoretical and experimental investigations for thermoelectric applications.

Figure 2(a) also includes our calculated result for the total scaled electronic density of states (DOS) for the material of interest. The scaled total electronic density of states has two major regions, an s region and a p bonding region. For energies lower than -4 eV the s states contribute in total DOS majorly and for energies higher than -4 eV the p states are dominant. The electronic states of the valence electrons are formed by sp^3 hybrid orbitals so; the main contribution to these states comes from p orbitals. Moreover, figure 2(b) presents the electron localization function (ELF) of Si_{46}-VIII which affords characterization of bonds. The values of ELF depend on position and vary between zero and one ($0 \leq \mathrm{ELF} \leq 1$). $\mathrm{ELF} = 0$ coincides with electron-gas-like pair probability [51]. The ELF is used to identify binding and electron pairs in simple molecular systems. The iso value of $\mathrm{ELF} = 0.8$ was selected for visualization. As it can be seen from figure 2(b) there are significant values of ELF in interstitial regions, indicating the presence and strength of directional, covalent-type bonds.

We have also calculated the electronic formation energy E_f for the type-VIII Si_{46} clathrate. The electronic energy of formation refers to the electronic part of the formation energy with respect to the elements in their standard state. The electronic energy of formation was calculated from the equation:

$$\Delta H_{el}(Si_{46}) = E_{Si_{46}} - 46E_{Si} \tag{16}$$

Table 2. Predicted elastic constants C_{ij}, bulk B, shear G, factor of anisotropy (no unit), and Young's E, E_{100}, and E_{111} moduli in GPa, Poisson's ratios, longitudinal, transverse, and mean sound velocities in m s^{-1}, Debye temperatures in K and Grüneisen constants for Si_{46}-VIII and Si_{46}-I (from [3]).

Type-VIII clathrate	Si_{46}-VIII	Si_{46}-I[a]
C_{11} (GPa)	149.28	140
C_{12} (GPa)	49.22	47
C_{44} (GPa)	46.83	47
B (GPa)	82.57	78
G (GPa)	48.08	46
C_a	1.027	0.97
E (GPa)	120.80	115.33
E_{100} (GPa)	124.87	116
E_{111} (GPa)	118.15	118
ν	0.24	0.25
ν_L (m s^{-1})	8395	8149
ν_T (m s^{-1})	4807	4683
ν_s (m s^{-1})	5196	4931
θ_D (K)	549	551
Grüneisen parameter	1.25	—

[a] Extracted from [3].

in which E_{Si} is the electronic energy per Si atom in diamond structure. The formation energy determines if it is energetically favorable for a material to form in comparison with the solids formed by its constituents. We find that the formation energy for Si_{46}, is 7.84 kJ mol^{-1}. The positive value of formation energy for type-VIII clathrate Si_{46} predicts that this material is not more stable than its constituents and the chemical reaction of formation is endothermic. In fact, we predict that the formation reaction will not take place spontaneously and extra energy must be added to the system to initiate the reaction. We also computed the zero point energy ($\Delta H_{ZPE}(Si_{46}) = 5.66$ kJ mol^{-1}) and the change to finite T ($\delta\Delta H_T(Si_{46}) = 1.42$ kJ mol^{-1}) to obtain the standard enthalpy of formation ΔH_T at temperature T as

$$\Delta H_T(Si_{46}) = \Delta H_{el}(Si_{46}) + \Delta H_{ZPE}(Si_{46}) + \delta\Delta H_T(Si_{46}) \tag{17}$$

and see whether the Si_{46}-VIII is likely to form without adding heat or not. $\delta\Delta H_T(Si_{46})$ is calculated by an analogous expression with E_f replaced by $E_{ph} = \sum_q \hbar\omega_q n(\omega_q)$ [51]. E_{ph} is the phonon energy without the ZPE, and $n(\omega) = 1/(e^{\hbar\omega/kT} - 1)$. The result $\Delta H_{298} = 12.08$ kJ mol^{-1} demonstrates that our previous result considering the electronic energy alone does not change.

3.1. Elastic properties

The elastic properties of Si_{46}-VIII were calculated at its theoretical equilibrium volume. For this purpose, the strain values were set to 0.005. The eigenvalues of the elastic stiffness matrix were found to be (99.9, 247.75, 99.9, 187.2, 187.2, and 187.2) for Si_{46} indicating that the matrices are positive-definite, and that the clathrate crystal is mechanically stable. In table 2 the calculated values of the elastic constants, bulk, shear, and Young's moduli, factor of anisotropy, longitudinal, transverse, and mean sound velocities along

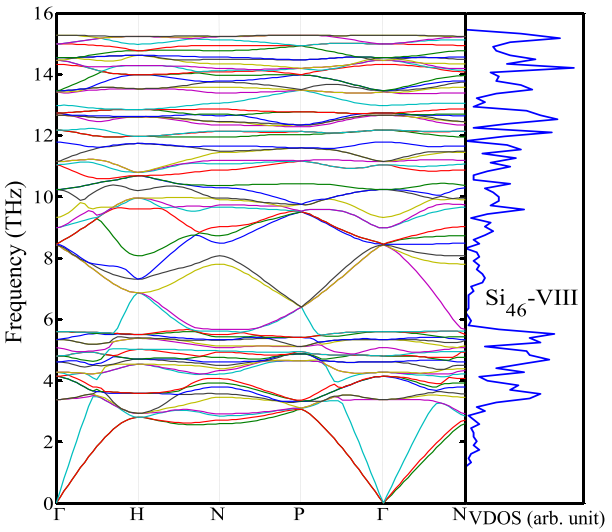

Figure 3. Calculated phonon dispersion relations and vibrational DOS for Si_{46}-VIII.

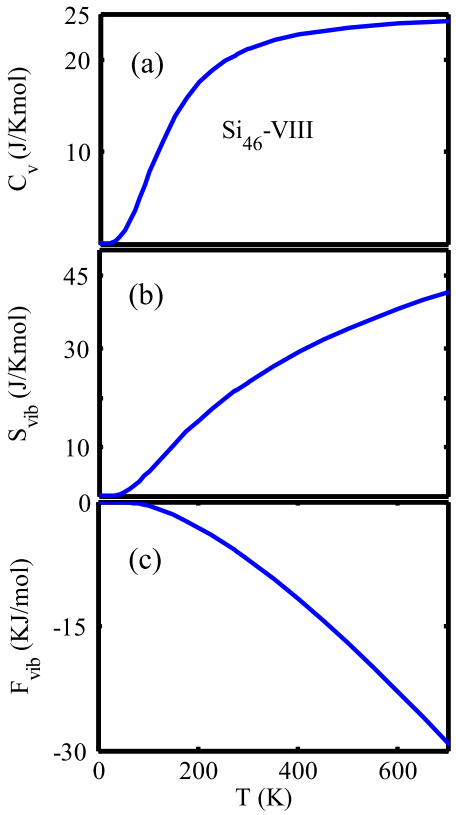

Figure 4. Calculated thermodynamic properties of Si_{46}-VIII, in the temperature range 0–700 K. (a) Heat at constant volume C_v, (b) vibrational entropy $S_{\rm vib}$, and (c) vibrational Helmholtz free energy $F_{\rm vib}$. The vertical axes are in logarithmic scale.

with Debye temperature for this material are listed. The corresponding values for clathrate Si_{46}-I were extracted and presented for comparison. The factor of anisotropy is close to 1 for clathrate Si_{46}-VIII. Therefore, according to strains, Si_{46}-VIII can be considered as a strongly isotropic material. Moreover, the Young's moduli have weak dependency on crystallographic directions. The Poisson's ratio which measures the stability of a crystal against shear was calculated as well. These results explain that similar to Si_{46}-I, Si_{46}-VIII is also stable against shear and under pressure.

3.2. Phonon spectra and vibrational density of states

The collective motion of all atoms in lattice is described in lattice dynamics by focusing on the vibrational eigenvalues or phonon spectra. Our calculated ground state phonon dispersion curves at $T = 0$ K along with their corresponding vibrational density of states (VDOS) are presented in figure 3 for the Si_{46}-VIII.

The acoustic modes are located below approximately 3.5 THz and the optical modes lie above that range. For Si_{46}-VIII, the acoustic mode curves have slopes almost as large as slopes of diamond silicon, indicating that the phonon group velocities in these two materials are comparable. There are two high densities of states regions in this material. One region is above the acoustic modes in the ranges of 3.5–5.8 THz, and the other region is near the top of the optical branch above 13 THz. Most of the optical mode curves are flat, which is reminiscent of zone folding. Thus, we expect that their contribution to heat transport will be small [52]. The highest optical mode is located at 15.5 THz.

A feature of the calculated VDOS is that it increases above both regions of acoustic and optic branches. The top of the acoustic bands is located at about 3 THz. As can be seen in figure 3, we also find gaps in both the phonon dispersion curves and the VDOS within the optic bands. The gaps are located in the ranges 11.82–11.96 THz and 12.18–12.42 THz. The existence of these gaps is unusual in covalently bonded materials and is a unique feature of clathrates possibly caused by the open structure and interconnected frameworks of their lattices [53]. In molecular solids, the high energy intramolecular modes (caused by the cage atoms) are separated from the low energy intermolecular modes (guest-cage modes), which results in these gaps.

3.3. Thermodynamic properties

Using the first principles and lattice vibrational results just discussed, we have calculated the vibrational contributions to the heat capacity at constant volume, the entropy, and the Helmholtz free energy in the Si_{46}-VIII clathrate in the temperature range 0–700 K. In the theory of the lattice dynamics, the heat at constant volume is more easily calculated than the heat at constant pressure, which is the more common experimentally measurable quantity. For solids, the two heats are related by $C_p - C_v = BTV\alpha_V^2$, where α_V is the volumetric coefficient of thermal expansion, B is the bulk modulus, T is the absolute temperature, and V is the volume. Figures 4(a)–(c) show our predicted temperature dependences of the heat, the vibrational entropy, and the vibrational Helmholtz free energy for Si_{46}-VIII system. The C_v curve in (a) increases smoothly with temperature in the range 0–300 K. At approximately 300 K, C_v begins to approach the Dulong and Petit value of $3NR$, where R is the gas constant and N is

the number of atoms in the unit cell. The C_v function flattens out as the temperature increases above about 300 K. This indicates that the optical and acoustic modes of this clathrate are all excited at room temperature. Our calculations predict that at $T = 300$ K, C_v for Si_{46}-VIII is 20.21 J K^{-1} mol^{-1}.

Figure 4(b) shows the predicted temperature dependences of the vibrational entropy of Si_{46}-VIII. The calculated vibrational entropy at $T = 300$ K is 20.17 J K^{-1} mol^{-1}. The entropy curves increases smoothly as the temperature increases. This behavior is expected because the vibrational frequencies should increase with temperature.

Figure 4(c) shows our calculated results for the vibrational Helmholtz free energy as a function of temperature for the Si_{46}-VIII material. The free energy of a material depends strongly on its geometrical structure.

4. Conclusions

The structural, electronic, vibrational, and thermodynamic properties of type-VIII clathrate Si_{46} were calculated from the first principles. GGA DFT was applied to investigate a wide range of properties of this clathrate and the results of these calculations were presented. The geometry of the clathrate was optimized before any other calculation. Our calculations predict that Si_{46}-VIII has an indirect bandgap. The predicted bandgap is about 1.24 eV. We also calculated the Grüneisen constant within the Grüneisen–Debye approximation for the Si_{46}-VIII. The calculated elastic constants have been used to predict the sound velocity and Debye temperature. Finally, we have calculated the temperature dependences of the vibrational heat, entropy, and the Helmholtz free energy of Si_{46}-VIII clathrate. Our calculations show that the temperature variations of these properties have similar characteristics as those found for other clathrate materials [54–56]. The electronic band structure predicts a large number of valleys located close to the valance band edge in Si_{46}-VIII which can enhance the thermoelectric power factor. With the improved power factor and the expected small thermal conductivity, due to its open framework structure, Si_{46}-VIII is predicated to make a good thermoelectric material, which deserves further theoretical and experimental investigation.

Acknowledgments

This work was partially supported by AFOSR under Grant no. FA9550-10-1-0010 and the National Science Foundation (NSF) under Grant no. 0933763. The authors would like to thank the Texas Tech and Oklahoma State Universities High Performance Computing Centers for many hours of computing time.

References

[1] Paschen S, Carrillo-Cabrera W, Bentien A, Tran V H, Baenitz M, Grin Y and Steglich F 2001 *Phys. Rev.* B **64** 214404
[2] Menon M, Richter E and Subbaswamy K R 2002 *Phys. Rev.* B **56** 12290
[3] Connétable D 2007 *Phys. Rev.* B **75** 125202
[4] Herrmann R F W, Tanigaki K, Kuroshima S and Suematsu H 1998 *Chem. Phys. Lett.* **283** 29–32
[5] Slack G A 1995 *CRC Handbook of Thermoelectrics* ed D M Rowe (Boca Raton, FL: CRC) p 407
[6] Myles C W, Biswas K and Nenghabi E 2007 *Physica* B **401/402** 695–8
[7] Myles C W, Dong J and Sankey O F 2003 *Phys. Status Solidi* b **239** 26–34
[8] Snyder G J and Toberer E S 2008 *Nature Mater.* **7** 105–14
[9] Nolas G S, Beekman M, Gryco J, Lamberton G A Jr, Tritt T M and McMillan P F 2003 *Appl. Phys. Lett.* **82** 910
[10] Fukuoka H, Kiyoto J and Yamanaka S 2003 *Inorg. Chem.* **42** 2933
[11] Imai M, Nishida K, Kimura T and Yamada K 2002 *J. Alloys Compounds* **335** 270
[12] Dong J and Sankey O F 1999 *J. Phys.: Condens. Matter* **11** 6129
[13] Nolas G S, Cohn J L, Dyck J S, Uher C and Yang J 2002 *Phys. Rev.* B **65** 165201
[14] Nolas G S, Vanderveer D G, Wilkinson A P and Cohn J L 2002 *J. Appl. Phys.* **91** 8970
[15] Biswas K and Myles C W 2007 *Phys. Rev.* B **75** 245205
[16] Biswas K and Myles C W 2006 *Phys. Rev.* B **74** 115113
[17] Sales B C, Chakoumakos B C, Jin R, Thompson J R and Mandrus D 2001 *Phys. Rev.* B **63** 245113
[18] Sasaki Y, Kishimoto K, Koyanagi T, Asada H and Akai K 2009 *J. Appl. Phys.* **105** 073702
[19] Kishimoto K, Ikeda N, Akai K and Koyanagi T 2008 *Appl. Phys. Express* **1** 031201
[20] Deng S, Saiga Y, Kajisa K and Takabatake T 2011 *J. Appl. Phys.* **109** 103704
[21] Madsen G K H, Schwarz K, Blaha P and Singh D J 2003 *Phys. Rev.* B **68** 125212
[22] Hohenberg P and Kohn W 1964 *Phys. Rev.* **136** B864
[23] Kohn W and Sham L J 1965 *Phys. Rev.* **140** A1133
[24] Perdew J P, Burke K and Ernzerhof M 1996 *Phys. Rev. Lett.* **77** 3865
[25] Baroni S, Giannozzi P and Testa A 1987 *Phys. Rev. Lett.* **58** 1861
[26] Gonze X 1997 *Phys. Rev.* B **55** 10337
[27] Gonze X and Lee C 1997 *Phys. Rev.* B **55** 10355
[28] Gonze X, Beuken J M, Caracas R, Detraux F, Fuchs M, Rignanese G M, Sindic L, Verstraete M, Zerah G and Jollet F 2002 *Comput. Mater. Sci.* **25** 478 (ABINIT is a common project of the Universite Catholique de Louvain, Corning Incorporated, and other contributors www.pcpm.ucl.ac.be/ABINIT)
[29] Hamann D R, Schluter M and Chiang C 1979 *Phys. Rev. Lett.* **43** 1494
[30] Troullier N and Martins J L 1991 *Phys. Rev.* B **43** 1993
[31] Payne M C, Teter M P, Allan D C, Arias T A and Joannopoulos J D 1992 *Rev. Mod. Phys.* **64** 1045
[32] Methfessel M and Paxton A T 1989 *Phys. Rev.* B **40** 3616
[33] Broyden C G 1970 *J. Inst. Math. Appl.* **6** 76
Fletcher R 1970 *Comput. J.* **13** 317
Goldfarb D 1970 *Math. Comput.* **24** 23
Shanno D F 1970 *Math. Comput.* **24** 647
[34] Haruna K, Meata H and Ohashi K 1987 *J. Phys. C: Solid State Phys.* **20** 5275
[35] Steigmeier E F and Abeles B 1964 Scattering of phonons by electrons in germanium–silicon alloys *Phys. Rev.* **136** A1149–55
[36] Hamann D R, Wu X, Rabe K M and Vanderbilt D 2005 *Phys. Rev.* B **71** 035117
[37] Le Page Y and Saxe P 2001 *Phys. Rev.* B **63** 174103
[38] Hill R 1952 *Proc. Phys. Soc. Lond.* **65** 349

[39] Vitos L 2007 *Computational Quantum Mechanicals for Materials Engineers* (London: Springer)
[40] Ledbetter H M 1973 *J. Appl. Phys.* **44** 1451
[41] Grimvall G 1999 *Thermophysical Properties of Materials* (Amsterdam: North-Holland)
[42] Toxvaerd S 1997 *J. Chem. Phys.* **107** 5197
[43] Jepson O and Andersen O K 1971 *Solid State Commun.* **9** 1763
[44] Lehmann G and Taut M 1972 *Phys. Status Solidi* b **54** 469
[45] Dong J J, Sankey O F, Ramachandran G K and McMillan P F 2000 *J. Appl. Phys.* **87** 7726
[46] Hull R 1999 *Properties of Crystalline Silicon* (London: INSPEC)
[47] Pei Y, LaLonde A D, Wang H and Snyder G J 2012 *Energy Environ. Sci.* **5** 7963–9
[48] Ure R W Jr and Heikes R R 1961 *Thermoelectricity; Science and Engineering* ed R P Helkes and R W Ure Jr (New York: Interscience)
[49] Pei Y, Wang H and Snyder G J 2012 *Adv. Mater.* **24** 46
[50] Shoemake G E, Rayne J A and Ure R W Jr 1969 *Phys. Rev.* **185** 1046
[51] Herbst J F and Hector L G Jr 2005 *Phys. Rev.* B **72** 125120
[52] Ashcroft N W and Mermin N D 1976 *Solid State Physics* (New York: Holt, Reinhart and Winston) p 500
[53] Kahn D and Lu J P 1997 *Phys. Rev.* B **56** 13898
[54] Bentien A, Johnsen S and Iversen B B 2006 *Phys. Rev.* B **73** 094301
[55] Qiu L, Swainson I P, Nolas G S and White M A 2004 *Phys. Rev.* B **70** 035208
[56] Qiu L, White M A, Li Z, Tse J S, Ratcliffe C I, Tulk C A, Dong J and Sankey O F 2001 *Phys. Rev.* B **64** 024303